

# Bidirectional transport and pulsing states in a multi-lane ASEP model

Congping Lin<sup>1,2</sup>, Gero Steinberg<sup>2</sup> and Peter Ashwin<sup>1</sup>

<sup>1</sup> Mathematics Research Institute, University of Exeter, Exeter EX4 4QF, UK

<sup>2</sup> Department of Biosciences, University of Exeter, Exeter EX4 4QD, UK

E-mail: E-mail: cl336@exeter.ac.uk, P.Ashwin@exeter.ac.uk and  
G.Steinberg@exeter.ac.uk

**Abstract.** In this paper, we introduce an ASEP-like transport model for bidirectional motion of particles on a multi-lane lattice. The model is motivated by experiments on organelle motility along a microtubule (MT), where particles are propelled by molecular motors (dynein and kinesin) along the thirteen protofilaments of the MT. In the model, particles can switch directions of motion due to “tug-of-war” events between counteracting motors. Collisions of particles on the same lane can be cleared by switching to adjacent filaments (lane changes).

We analyze transport properties of the model with no-flux boundary conditions at the end of a MT (“plus-end” or tip). In particular, we find a nonlinear scaling of the mean number of particles accumulated at the tip (*tip size*) with injection rate and an associated phase transition leading to *pulsing states* characterized by periodic filling and emptying of the system. Moreover, we show that the ability of changing protofilaments can affect the transport efficiency. Finally, we show that the particle-direction change rate obtained from experiments is close to optimal in order to achieve efficient motor and organelle transport in a living cell.

**Keywords:** traffic and crowd dynamics, molecular motors (theory), stochastic particle dynamics (theory), phase transition

## 1. Introduction

The cytoplasm of living cells contains a complex network of fibres, the cytoskeleton which helps to maintain cell shape by providing structural support and mediating transport within the cell. Bidirectional transport is mediated by specialized mechano-proteins, so-called molecular motors, that utilize ATP to move vesicles, organelles or other cargo along the cytoskeleton [1]. Microtubules (MTs) are one type of cytoskeletal elements that consist of thirteen oriented protofilaments [2] (which we refer as *lanes*), each of which can support bidirectional transport. Long-distance transport along MTs is powered by kinesin and dynein. Kinesin takes its cargo to the polymerization-active plus-end of a MT while dynein walks towards minus-ends [1].

Various models [3, 4, 5, 6, 7] have been developed to describe and understand unidirectional transport. Recently, to investigate bidirectional transport, a two-lane model involving bidirectional traffic on the same lane with detachment and attachment associated with another lane is considered [8, 9, 10]; bidirectional motion on a single lane with site sharing is also investigated [11]; in addition, a two-lane asymmetric simple exclusion process (ASEP) model where particles walking in different directions move on different lanes is discussed in [12, 13, 14]. With robust quantitative data of motor behaviour in long-range motility derived from live-imaging of cells, a two-lane model in [14] and a subsequent modelling approach in [15] are used to investigate molecular basis of motor accumulation at the MT tip. This led to the conclusion that a significant number of motors accumulate at MT plus-ends in a stochastic way [15]. A major advantage of the modelling in [15] is that the model considers thirteen protofilaments and that motors can change filaments along a MT. The lane-change rules assumed in [15] are based on experimental observations that (a) dynein can switch between lanes on the MT at a certain rate [16], whereas (b) kinesin remains on a single lane [17], and (c) no long-lasting traffic jam is observed between particles away from the tip. However, more recent reports show that kinesin has the capacity to change lanes to overcome permanent obstacles on the MT [18]. Thus the situation in the living cell is less clear.

In this paper, we investigate the effect of different lane-change rules (that is which particles can change lanes) on bidirectional transport. This includes a diffusion between lanes and the effect on possible measures of bidirectional transport efficiency. We find that the *in vivo* parameters obtained in living cell from [15] indicate a close-optimal for effective bidirectional transport with regards to a balance between arrival proportion and the ratio of delay at the tip. By changing parameters, we find nonlinear behaviour of the mean tip size with injection rate and a singularity at a finite injection rate which is related to a novel *pulsing state*.

The paper is organized as follows: in Section 2 we introduce a general  $M$ -lane ASEP model for bidirectional motion. Section 3 examines lane-change influences on the bidirectional transport while Section 4 examines some novel *pulsing states* with whole-system filling and emptying that can appear at injection rates beyond the singularity. We finish with a discussion of the biological relevance, implications and generalizations of the model in Section 5.

## 2. A multi-lane model for bidirectional transport

Motivated from the *in vivo* observations and the thirteen-lane model discussed in [15], we introduce a general multi-lane bidirectional ASEP model where particles move on a lattice of spatial locations consisting of  $M$  adjacent lanes around the circumference of a cylinder<sup>‡</sup>. Each lane is discretized into  $N$  sites between oriented *plus-ends* and *minus-ends*, as illustrated in Figure 1. Particles are of two types; *plus-type* particles go towards the plus-end while *minus-type* particles go towards the minus-end; these

<sup>‡</sup> We identify lane  $M + 1$  with lane 1 to represent this cylinder.

particles represent a single load of motor proteins that permanently bound to the load and pulled along the lane by only one type of the motors in bound to the MT.

We identify each location along the cylinder by a pair  $(l, i)$  where  $l \in \{1, \dots, M\}$  denotes the lane and  $i \in \{1, \dots, N\}$  the site along the lane. We let  $\tau_{\pm, i}^l = 1$  or 0 represent the presence or absence of a plus-type (minus-type) particle at location  $(l, i)$ . Each location is occupied by at most one particle (i.e.  $\tau_{+, i}^l + \tau_{-, i}^l$  can only be 0 or 1) and particles move from one location to another at given rates. In addition we allow the possibility that each particle can change from one type to the other at rates representing the resolution of brief “tug-of-war” events [19, 20, 21, 22] between opposite oriented motor proteins bound to the particle. This change of type may or may not be associated with a change of lane.

Plus- and minus- type particles have different transition rates between locations and these transition rates, including *motion* and *particle type change* (see below) rates in the model are independent of site (site homogeneity§), though we do include the possibility that these rates depend on lane (lane inhomogeneity). We say a model is *lane-inhomogeneous* (or simply *inhomogeneous*) if the transition rates and/or boundary conditions are not uniform between lanes; otherwise we say the model is (lane) *homogeneous*. A plus-type particle at location  $(l, i)$  is *unblocked* if  $\tau_{+, i+1}^l + \tau_{-, i+1}^l = 0$ , otherwise it is *blocked*; similar to minus-type particles. Transition rates may depend on whether a particle is blocked or not as illustrated in Figure 1 and possible transitions are defined as the following:

- **Motion:** Plus-type particles move from  $(l, i)$  to  $(k, i + 1)$  with a change of lane  $l$  to  $k$  when unblocked (resp. blocked) at rate  $p_{+, u}^{l \rightarrow k}$  (resp.  $p_{+, b}^{l \rightarrow k}$ ). Similarly, minus-type particles move from  $(l, i)$  to  $(k, i - 1)$  at rate  $p_{-, u(b)}^{l \rightarrow k}$ . Motion is subject to an exclusion principle - a change can only occur if the target location to move into is vacant. **Forward motion** is used to mean the motion on a single lane (i.e.,  $k = l$ ) in either direction. This can occur only when unblocked and for lane-homogeneous forward motion we write

$$p_+ := p_{+, u}^{l \rightarrow l}, \quad p_- := p_{-, u}^{l \rightarrow l}.$$

- **Particle type/direction change:** Plus-type particles can change to minus-type particles with a change of lane  $l$  to lane  $k$  at rate  $p_{+-}^{l \rightarrow k}$ . Minus-type particles can change to plus-type particles with a similar change in lane at rate  $p_{-+}^{l \rightarrow k}$  (we assume that the site  $i$  is preserved for a change in type). For lane-homogeneous direction changes on the same lane, we write

$$p_{+-} := p_{+-}^{l \rightarrow l}, \quad p_{-+} := p_{-+}^{l \rightarrow l}.$$

Boundary conditions for the model are assumed as follows:

§ We refer to *site homogeneity* if the rates of transition in relation to any location  $(l, i)$  are independent of  $i$  for each  $l \in \{1, 2, \dots, M\}$ .

- **Inflow:** Plus-type particles are injected at rate  $\alpha_+^l$  into the minus end of the  $l$ -th lane, while minus-type particles are injected at rate  $\alpha_-^l$  into the plus end of the  $l$ -th lane, in both cases subject to an exclusion principle.
- **Outflow:** Plus-type particles exit from the plus end of the  $l$ -th lane at rate  $\beta_+^l$ , while minus-type particles exit from the minus end of the  $l$ -th lane at rate  $\beta_-^l$ .

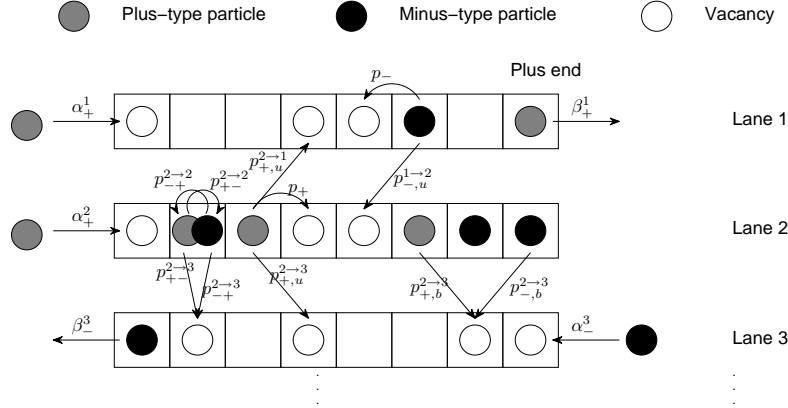


**Figure 1.** Schematic diagram showing transition rates for the multi-lane bidirectional ASEP model. The plus end (resp. minus end) of the MT is at the right (resp. left). Plus-type (resp. minus-type) particles move step forward with rate  $p_+$  (resp.  $p_-$ ) while they move forward associated with a change of lane with rates  $p_{+,b(u)}^{l \rightarrow l \pm 1}$  (resp.  $p_{\pm,b(u)}^{l \rightarrow l \pm 1}$ ) when blocked (resp. unblocked). Plus-type (resp. minus-type) particles are injected into the left (resp. right) boundary of the system at rate  $\alpha_+^l$  (resp.  $\alpha_-^l$ ) and exit at rate  $\beta_+^l$  (resp.  $\beta_-^l$ ) in the  $l$ -th lane. Particles can also change from plus-type to minus-type (resp. from minus-type to plus-type) with rate  $p_{+-}^{l \rightarrow k}$  (resp.  $p_{-+}^{l \rightarrow k}$ ) associated with a possible change of lane  $l$  to  $k$  (if  $l \neq k$ ); we assume the site is preserved during a change of type.

The state of the model  $\{\tau_{\pm,i}^l(t)\}$  at time  $t$  changes according to the above events (assumed to take place independently and instantaneously) from an initial state  $\{\tau_{\pm,i}^l(0)\}$ . In summary, the model for a given lattice (fixed  $M$  and  $N$ ) has a number of parameters

$$p_{\pm,b}^{l \rightarrow k}, p_{\pm,u}^{l \rightarrow k}, p_{+-}^{l \rightarrow k}, p_{-+}^{l \rightarrow k}, \alpha_{\pm}^l \text{ and } \beta_{\pm}^l$$

for  $k, l = 1, \dots, M$  that collectively determine the bidirectional transport behaviour. We write  $\alpha_+ = \sum_{l=1}^M \alpha_+^l$  to denote the total inflow of plus-type particles. In practice, many of these rates will be zero - for example, here we only permit a type change of a particle that remains on the same lane or moves to an adjacent lane. As other ASEP models, we assume that the dynamics for typical choices of parameters converges to a unique statistical equilibrium independent of initial conditions, though possibly after a long transient. Exceptions occur if there is a degeneracy of the parameters, for example if no lane-changes are permitted, i.e.,  $p_{\pm,b(u)}^{l \rightarrow k} = 0$  for  $k, l = 1, \dots, M$ , then accumulations can be created at arbitrary locations that are never cleared. The system exhibits various different dynamical regimes depending on parameters. We have not

**Table 1.** The transition rates (a) with boundary conditions I in (b) for a two-lane model  $M = 2$  that gives bidirectional transport where each lane supports transport in one direction only and allows lane changes only together with a type change; If also associated with boundary Conditions II, the model with  $M = 2$  corresponds to no-flux boundary at the plus end.

(a) Transport rates	
$p_{-+}^{l \rightarrow l} = p_{+-}^{l \rightarrow l} = 0, \quad p_{\pm, u(b)}^{l \rightarrow l \pm 1} = 0 \quad (l = 1, 2), \quad p_d := p_{+-}^{1 \rightarrow 2}, \quad p_u := p_{-+}^{2 \rightarrow 1}, \quad p_{\pm} := p_{\pm, u}^{l \rightarrow l}$	
(b) Boundary conditions I	Boundary conditions II
$\alpha_+^2 = \alpha_-^1 = 0$	$\beta_+^1 = \alpha_-^2 = 0$

attempted to characterize the phase diagram of these states in full, but we highlight novel pulsing and filled states in section 4.1.

The equilibrium densities of plus- and minus-type particles are defined to be the mean occupancy of the particles:

$$\rho_i^l := \langle \tau_{+,i}^l(t) \rangle, \quad \sigma_i^l := \langle \tau_{-,i}^l(t) \rangle. \quad (1)$$

where  $\langle \cdot \rangle$  denotes the ensemble average; assuming ergodicity this can be evaluated using a time average. In particular, if there is an accumulation at the tip - we denote the *lane tip length*  $\lambda_{tip}^l(t)$  as the number of particles in the accumulation within lane  $l$  at time  $t$ , and the tip size  $n_{tip}(t)$  is

$$n_{tip}(t) = \sum_{l=1}^M \lambda_{tip}^l(t).$$

with mean tip size as  $\langle n_{tip} \rangle$  at stead state.

There are few methods giving exact analytical solutions of the equilibrium state for ASEP models (we refer to [4] for a review of ASEP models and their analytical solution). Therefore, we numerically simulate this discrete event, continuous time model using both Gillespie [23] and fixed time-step ( $h_t$ ) Monte Carlo methods. The latter method converges to the Gillespie method and gives outcomes that are independent of update methods in the limit  $h_t \rightarrow 0$ .

When switching off the particle-type change rates, i.e.  $p_{+-}^{l \rightarrow k} = p_{-+}^{l \rightarrow k} = 0$  for  $k, l = 1, 2, \dots, M$  and the inflow of minus-type particles, i.e.,  $\alpha_-^l = 0$ , the model is similar to the ASEP models in [3, 4]. In the following subsections, we show that when allowing particle-type changes, the model introduced above can limit in special cases to the two-lane model in [12, 13, 14] and the thirteen-lane model in [15].

### 2.1. A simple two-lane model

For two lanes ( $M = 2$ ), setting the parameters satisfying Table 1 (a) with boundary conditions I in Table 1 (b) corresponds to the two-lane model in [12, 13]. This particular choice of parameters segregates the particles into two lanes of unidirectional motion- one lane will have no particles of minus-type, while the other lane will have no particles of

plus-type, i.e., the equilibrium densities  $\rho^2 = \sigma^1 = 0$ . If further satisfying boundary conditions II in Table 1 (b), then there is no flux at the right boundary and the model corresponds to the special case studied in [14]. We recall from [14] that in these circumstances with minus-end boundary condition  $\alpha_+^1 = \alpha_+$  small enough on the first lane and  $\beta_-^2 = p_-$  on the second lane, a shock forms near the tip that traps a number of particles; using a mean-field approximation and denote  $x = i\delta$  where  $\delta = 1/N$ , one can find an asymptotic profile for the equilibrium densities of  $\rho$  and  $\sigma$  for plus- and minus-type particles along the domain as follows (assuming  $\sigma^2$  and  $\min\{\rho^1, (1 - \rho^1)\}$  are in order of  $\delta$ ):

$$\rho^1(x) \approx \begin{cases} \frac{\alpha_+}{p_+} \exp\left[x\left(\frac{Np_u}{p_-} - \frac{Np_d}{p_+}\right)\right], & x \in [0, x_s] \\ 1 + \frac{p_d N}{p_+}(x - 1), & x \in [x_s, 1] \end{cases}, \quad (2)$$

$$\sigma^2(x) = \begin{cases} \rho^1(x), & x \in [0, x_s] \\ 1 - \rho^1(x), & x \in [x_s, 1] \end{cases}, \quad (3)$$

where  $x_s$  represent the shock location; continuity of the current then implies that the *mean tip size* can be approximated as

$$\langle n_{tip} \rangle \approx (1 - x_s)N \approx \frac{\alpha_+}{p_d} \exp\left(\frac{Np_u}{p_-} - \frac{Np_d}{p_+}\right). \quad (4)$$

## 2.2. A homogeneous thirteen-lane model

Taking  $M = 13$  and considering lane-homogeneous transition rates satisfying Table 2 (b) and explicit values as in Table 2 (a), the multi-lane model gives the thirteen-lane model discussed in [15]. If we consider boundary conditions

$$\alpha_+^l = \alpha_+/M, \quad \alpha_-^l = 0, \quad \beta_+^l = 0 \quad \text{and} \quad \beta_-^l = p_+ \quad (5)$$

for all  $l \in \{1, \dots, M\}$ , this corresponds to homogeneous injection of plus-type particles into the minus-end, no flux at the plus-end of the domain while minus-type particles exit without impediment. Experiments and other information reported in [15] suggest the rates listed in Table 2 (a). Rates in Table 2 as well as the boundary conditions in (5) are considered as default parameters here unless otherwise specified. In this paper we investigate various changes of these rates and meanwhile, we show in Section 3.1 that the model suggests very similar asymptotic formula of the density to those obtained for the two-lane model, at least for dilute states.

## 3. Influence of collisions and lane-changes on transport properties

In this section, we consider the multi-lane model lane-homogeneous transition rates satisfying Table 2 (b) and with boundary conditions in (5) except for possibly inhomogeneous injection rates. For lane-homogeneous lane changes, we write

$$p_{+,u(b)}^\downarrow := p_{+,u(b)}^{l \rightarrow l+1}, \quad p_{+,u(b)}^\uparrow := p_{+,u(b)}^{l \rightarrow l-1}$$

**Table 2.** Transition rates for the thirteen-lane model based on *in vivo* experiment measurements or estimations of velocities, mean run length and fluxes on a MT as detailed in [15] relative to a space step  $h_s = 0.008 \mu m$ . Here  $\alpha_+$  represents the total injection rate, i.e.,  $\alpha_+ = \sum_{l=1}^M \alpha_+^l$ . Simulations use  $N = 1250$  sites, i.e.,  $L = 10 \mu m$  in length discretised with the space step  $h_s$  and a sequential Monte-Carlo update with time step  $h_t = 0.0042$  s unless otherwise specified.

(a) Possible transition rates $s^{-1}$								
$p_+$	$p_-$	$p_{+,-}$	$p_{-,+}$	$p_{+,u}^{l \rightarrow l \pm 1}$	$p_{+,b}^{l \rightarrow l \pm 1}$	$p_{-,u}^{l \rightarrow l \pm 1}$	$p_{-,b}^{l \rightarrow l \pm 1}$	$\alpha_+$
212.5	203.83	0.0406	0.0273	0	0	4.335	106.25	1.06
(b) Only adjacent lane changes permitted					Type changes occur on a same lane			
$p_{\pm,b(u)}^{l \rightarrow k} = 0 \ (k \neq l, l \pm 1)$					$p_{-+}^{l \rightarrow k} = p_{+-}^{l \rightarrow k} = 0 \ (k \neq l)$			

and similarly for  $p_{-,u(b)}^\downarrow$  and  $p_{-,u(b)}^\uparrow$ . If the lane changes are also symmetric in two adjacent lanes, we remove the superscript and write

$$p_{+,u(b)} := p_{+,u(b)}^{l \rightarrow l \pm 1}, \quad p_{-,u(b)} := p_{-,u(b)}^{l \rightarrow l \pm 1}$$

independent of lane  $l$ .

### 3.1. Mean field approximation and cross-lane diffusion

In cases of inhomogeneous boundary conditions, the densities of plus- or minus-type particles can be homogenised by lane changes of particles, though clearly lane changes is necessary for this to happen. Depending on which particles change lane under which circumstances (blocked or unblocked), this homogenization can occur to one or both types of particle.

For example, if only minus-type particles can change lanes as in Table 2 in dilute situation, the density of minus-type becomes lane-homogeneous by cross-lane diffusion (see case (c) in Figure 2), while the density of plus-type particles (not shown) may still be inhomogeneous due to the inhomogeneous injection rates and no lane changes of this type. Additionally, the density of both type of particles can be more homogeneous than initially lane-inhomogeneous density by lane changes of plus-type particles (see case (b) in Figure 2 for the density profile of plus-type particles); the density of minus-type particle (not shown) is also more homogeneous than initially density and this is due to the homogeneous accumulation of plus-type particles along each lane at the plus end. Exceptions to this, shown in case (a1) and (a2), are when the both type of particles cannot change lanes, in which case the plus-type particles injected into the middle lane “sweep” that lane clear of minus-type particles.

These effects can be understood in terms of cross-lane diffusion of particles induced by lane changes in the dilute system. If we apply the mean field description of Appendix A to the dilute system and assume small variation of density with site location  $x = i\delta$  ( $x \in [0, 1]$  and  $\delta = 1/N$ ), in the case of  $p_{-,u} = p_{+,u} = 0$ , the solutions (A.1) and (A.2) in Appendix A.1 indicate the non-homogeneity of densities in

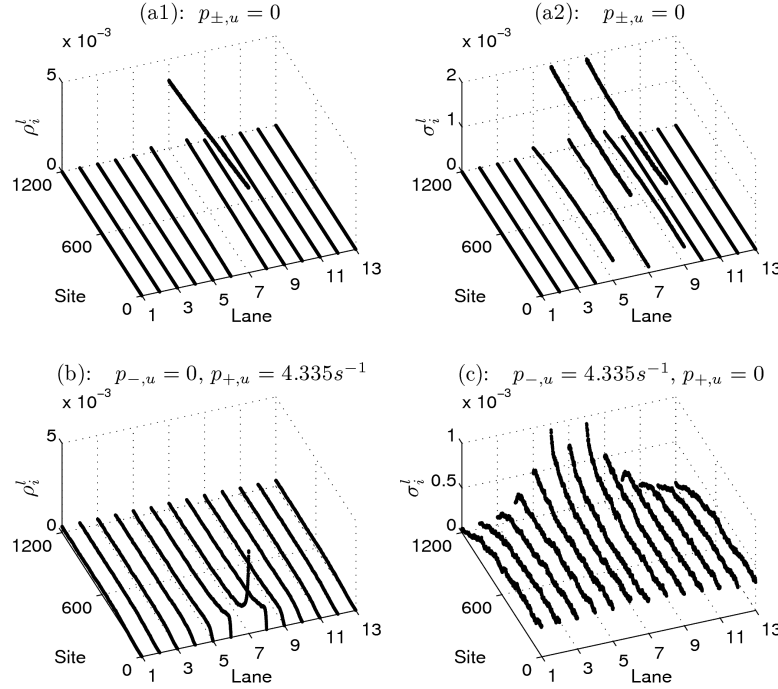


**Figure 2.** Densities of plus- or minus-type particles corresponding to default parameters in Table 2 and boundary conditions in (5) except that the lane-change rates when unblocked are varied and there is injection in only one lane (namely  $\alpha_+^7 = 1 \text{ s}^{-1}$  and  $\alpha_+^l = 0$  for  $l \neq 7$ ). (a1) and (a2) show the inhomogeneous densities of plus- and minus-type particles respectively, when particles only change lanes after collisions; case (b) (resp. (c)) shows cross-lane diffusion leading to a more homogeneous density of plus-type (resp. minus-type) particles away from the boundaries with lane-change rates when unblocked as indicated. In all cases the densities near the tip (not shown) are high.

both type particles if given non-homogeneous injection rates  $\alpha_+^l$ ; allowing lane changes in unblocked case, assuming that a change of type occur more slowly than a change of lane, i.e.,  $p_{-+}, p_{+-} \ll p_{\pm,u}$ , then the stationary state distribution  $\rho^l(x)$  satisfies (see Appendix A.1 for details):

$$0 = -\delta p_+ \frac{d\rho^l}{dx} + p_{+,u} \left[ \rho^{l-1} + \rho^{l+1} - 2\rho^l - \delta \frac{d\rho^{l-1}}{dx} - \delta \frac{d\rho^{l+1}}{dx} \right] \quad (6)$$

to leading order in  $\delta$ . Solving this differential-difference equation for  $M$  lanes gives

$$\rho^l(x) = \sum_{k=0}^{\lfloor M/2 \rfloor} \left[ A_k \cos \frac{2\pi k l}{M} + B_k \sin \frac{2\pi k l}{M} \right] \exp[-\kappa_+(k)x]$$

where

$$\kappa_+(k) = \frac{2p_{+,u} \left[ 1 - \cos \frac{2\pi k}{M} \right]}{\delta p_+ + 2p_{+,u} \delta \cos \frac{2\pi k}{M}},$$



and  $A_k, B_k$  are constants determined by the density at  $\rho^l(x_0)$ . Similarly, the density for the minus-type particles can be approximated as

$$\sigma^l(x) = \sum_{k=0}^{\lfloor M/2 \rfloor} \left[ A'_k \cos \frac{2\pi kl}{M} + B'_k \sin \frac{2\pi kl}{M} \right] \exp [\kappa_-(k)x]$$

where

$$\kappa_-(k) = \frac{2p_{-,u} \left[ 1 - \cos \frac{2\pi k}{M} \right]}{\delta p_- + 2p_{-,u} \delta \cos \frac{2\pi k}{M}}.$$

and  $A'_k, B'_k$  are constants determined by  $\sigma^l(x_0)$ . This suggests, not surprisingly, that the main effect of the lane-change in dilute cases is simply a diffusion of the density across the lanes in the direction of travel.

Assuming there is a unique equilibrium state, the density for plus- and minus-type particles in the multi-lane model with homogeneous rates as in Table 2 will have lane homogeneity though it will depend on site. For large enough  $\alpha_+$ , dynamically pulsing states as discussed later in Section 4.1 will appear, but for small  $\alpha_+$ , the system tends to a stationary state that is dilute near the minus end and dense near the plus end. Using similar methods as detailed in Appendix A to the lane-homogeneous case [14], for small injection rate, under the conditions that  $\rho, \sigma = O(\delta)$  far away from the tip and ignoring  $O(\delta^2)$ , we find similar approximate expressions as (2) for the stationary state in dilute regions; see (A.3).

### 3.2. A phase transition in the tip accumulation

For the half-closed system (i.e. closed at the plus end) in both the two-lane and thirteen lane models, it is clear that for typical particle-type change rates (e.g.,  $p_{+-} \ll p_+$ ), particles accumulate at the tip. On the other hand, from the mean tip size approximation (4) for the two-lane model, we see that  $\langle n_{tip} \rangle$  increase linearly with injection rate  $\alpha_+$ . However, it is not the case in a more general multi-lane (say,  $M = 13$ ) model. In the following, we investigate the size of the tip accumulation and its dependence on the total injection rate  $\alpha_+$  for the thirteen-lane model with otherwise default parameters as in Table 2 and boundary conditions as in (5).

We simulate two lane-change protocols PI and PII. The protocol PI only allows minus-type particles to change lanes while protocol PII allows both type to change lanes when blocked; lane-change rates are assumed homogeneous and symmetric (see detailed description in Section 3.3). Simulations gave a mean tip size that depends on  $\alpha_+$ , fitting to a rational function with three fitting parameters  $A, B$  and  $C$

$$\langle n_{tip}(\alpha_+) \rangle = \frac{\alpha_+ A (1 + \alpha_+ C)}{1 - \alpha_+ B};$$

see Figure 3 and Table 3. From the rational fitting function, when  $\alpha_+$  goes to the critical injection rate  $\alpha_c = 1/B$ , the mean tip size tends to infinity if the system can maintain steady (this may be possible for an infinite system). For the simulated system, the

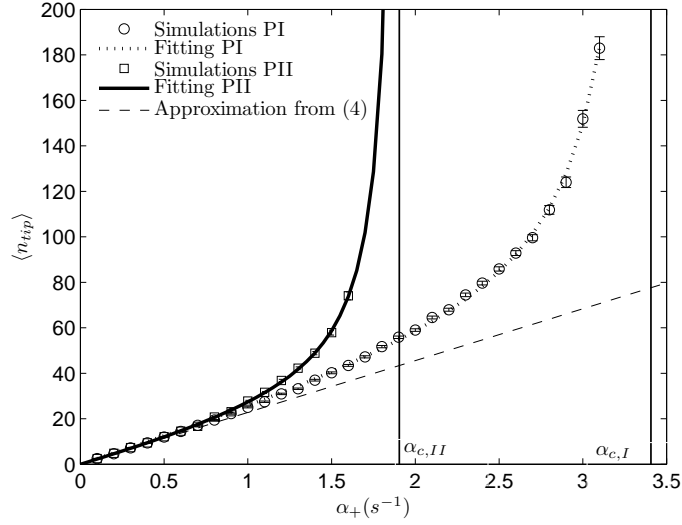


**Figure 3.** Mean tip size as a function of total injection rate  $\alpha_+$  for the thirteen-lane model with parameters otherwise as in Table 2 and boundary conditions in (5). Simulations PI refers to lane-change protocol PI where  $p_{-,b} = p_+/2$  and  $p_{+,b} = 0$  while simulations PII is for protocol PII where  $p_{\pm,b} = p_+/2$ . In both cases we find a good fit to a rational function of  $\alpha_+$  with a singularity at a critical value  $\alpha_{c,I} \approx 3.406 \text{ s}^{-1}$  (fitting PI) or  $\alpha_{c,II} \approx 1.947 \text{ s}^{-1}$  (fitting PII). For comparison, the straight dash line shows a linear dependence (4) of  $\alpha_+$  in the two-lane model recalled in Section 2.1; other parameters use the values of corresponding rates in Table 2; see [14] for details.

**Table 3.** Best fit of the data from simulations in Figure 3 to a rational function  $\langle n_{tip}(\alpha_+) \rangle = \frac{\alpha_+ A(1 + \alpha_+ C)}{1 - \alpha_+ B}$  with parameters  $A, B, C$ . The values indicate best fit values and standard errors.

	A	B	C
PI	$24.45 \pm 0.329$	$0.2936 \pm 0.00139$	$-0.2525 \pm 0.00388$
PII	$22.18 \pm 0.509$	$0.5136 \pm 0.00908$	$-0.3978 \pm 0.002219$

critical values are  $\alpha_{c,I} = 3.406 \text{ s}^{-1}$  and  $\alpha_{c,II} = 1.947 \text{ s}^{-1}$  respectively for lane-change protocol PI and protocol PII. For larger  $\alpha_+$  (near or beyond the critical value) in a finite system, we find a new phase of motions - the *pulsing state* examined in Section 4.1; see Figure 8. Additionally, by comparison to approximation (4) for a two-lane model, we note that the mean tip size in the thirteen-lane model increase in a similar tendency before  $\alpha_+ \approx 1$  (where  $\langle n_{tip} \rangle \approx 2 \times 13$ ), and starts to increase nonlinearly after that value.

This nonlinear increase of the mean tip size against injection rate in both lane-change protocols and their difference are further investigated by looking at the structure of accumulation and trapped percentage of minus-type particles at the tip in the following subsection.

### 3.3. Influence of lane-changes on the tip accumulation

The size of accumulation at the tip clearly depends on the lane-change rules (see Figure 3). Recall from Section 3.1 that lane changes can homogenize the densities so we expect the homogeneity of  $\lambda_{tip}^l(t)$  among the lanes will depend on the lane-change rules when blocked. To confirm this, we examine the maximum difference among the  $\lambda_{tip}^l(t)$  defined as

$$\Delta\lambda_{tip}(t) = \max\{\lambda_{tip}^l(t) - \lambda_{tip}^k(t) : k, l = 1, \dots, M\}.$$

The distribution of this quantity gives a measure that characterizes how “smooth” ( $\Delta\lambda_{tip}$  small) or “ragged” ( $\Delta\lambda_{tip}$  large) the tip is. In particular, the larger the mean value  $\langle\Delta\lambda_{tip}\rangle$ , the easier it is for minus-type particles to be released from the tip.

We consider four different lane-change (when blocked) protocols with homogeneous lane-change rates in an attempt to better understand their influence on the structure of tip accumulation via the distribution of  $\Delta\lambda(t)$  at stationary state. These are:

- (PI)  $p_{-,b} = p_+/2$ ,  $p_{+,b} = 0$  – only minus-type particles are allowed to change lanes with a rate (homogeneous and symmetric) that preserves the velocity; this corresponds to the assumption used in [15].
- (PII)  $p_{\pm,b} = p_+/2$  – both minus- and plus-type particles are allowed to change lanes;
- (PIII)  $p_{-,b} = 0$ ,  $p_{+,b} = p_+/2$  – only plus-type particles are allowed to change lanes;
- (PIV)  $p_{-,b}^\uparrow = p_+/2$ ,  $p_{-,b}^\downarrow = 0 = p_{+,b}$  – only minus-type particles are allowed to change and to only one of the adjacent lanes.

We ignore lane changes in the unblocked case as these are clearly not significant for escape from the tip. The distributions of the length differences  $\Delta\lambda_{tip}$  at a fixed stationary time are shown in Figure 4 for above four different lane-change protocols; other rates are as default ones. Note that allowing plus-type particles to undertake lane changes “smooths” the structure of the tip. The results for lane-change protocols PI and PII agree with the homogenized density of both type of particles on the effect of lane changes (see Figure 2). Note the similar distribution of  $\Delta_{tip}$  between PI and PIV (PII and PIII) from Figure 4, it is then reasonable to consider protocols PI and PII as typical lane-change protocols.

For both lane-change protocols PI and PII, particles can be trapped under several layers in the tip accumulation. Shown in Figure 3 that the mean tip size increases more rapidly with injection rates for protocol PII, We suggest this is due to there being more minus-type particles “trapped” in the tip which in turn lead to larger increase on the tip size. We say a particle is “trapped” if its motion (including forward motion and lane changes) is obstructed by occupation of other particles and loss the ability to take the motion due to the exclusion principle. We define two fractions: the *trapped minus-type fraction*  $F_{-,trap}$  and the *minus-type fraction* within the tip  $F_-$  in the steady state as

$$F_{-,trap} = \frac{\text{mean number of “trapped” minus-type particles at the tip}}{\text{mean number of total minus-type particles at the tip}},$$

$$F_- = \frac{\text{mean number of total minus-type particles at the tip}}{\langle n_{tip} \rangle}.$$

In the two-lane model recalled in Section 2.1, two types of particles move on different lanes and the density profile of minus-type particles is dilute, which indicates  $F_{-,trap} \approx 0$ . Additionally, from expressions (2) and (3),

$$F_- \approx \int_{x_s}^1 \sigma(x) dx / \int_{x_s}^1 (\rho(x) + \sigma(x)) dx \approx \frac{p_d}{2p_+} \langle n_{tip} \rangle$$

For particular parameters as in Table 2 with  $p_d = p_{+-}$ , the minus-type fraction  $F_- \approx 0.2\%$  associated with a mean tip size  $\langle n_{tip} \rangle \approx 20$ . However, in the thirteen lane model, from Table 4, for low  $\alpha_+ = 0.8 \text{ s}^{-1}$  in lane-change protocol PI, there are  $F_- \approx 4\%$  associated with  $\langle n_{tip} \rangle \approx 20$  and  $F_{-,trap} \approx 40\%$ . This shows a difference between the two-lane model and the thirteen-lane model even for low injection rates, though with similar mean tip size. In the two-lane model, viewed as a queueing process, the expected delay for particles at the tip is  $1/p_{+-}$ , therefore, positive fraction of trapped minus-type agrees with later on discussion on an average delay time  $E_2 > 1/p_{+-}$  in Section 3.4.

Comparing between the two lane-change protocols from Table 4, protocol PI gives lower  $F_{-,trap}$  and  $F_-$  than those in protocol PII, with either the same  $\alpha_+$  or the same mean tip size. This agrees with that a smoother structure of the tip accumulation is more likely to trap minus-type particles at the tip and indicates that the tip size and the (trapped) minus-type fraction are affected by each other.

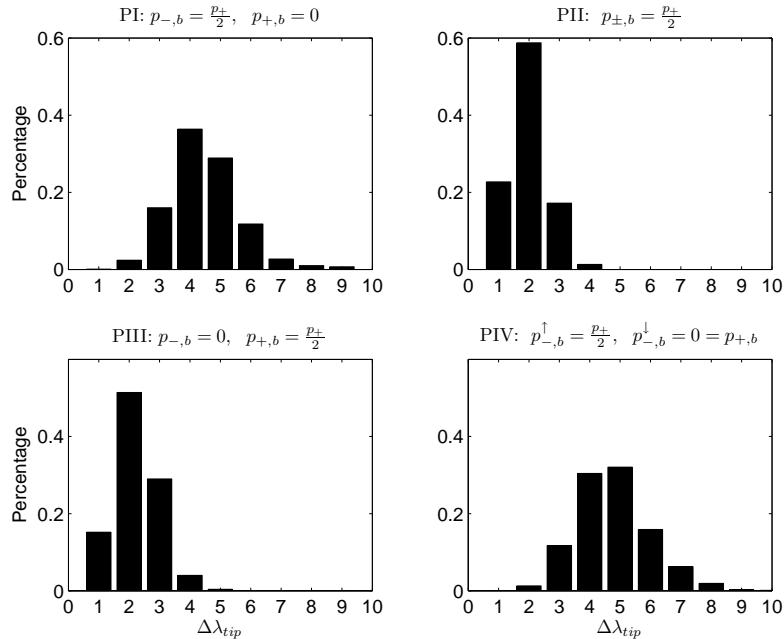


**Figure 4.** Distribution of maximum length difference  $\Delta\lambda_{tip}$  for lane-change protocols PI-IV; other parameters are default as in Table 2 and boundary conditions as in (5). Note that the structure of the tip accumulation in PII or PII is clearly smoother than that in PI and PIV.

**Table 4.** Comparison of trapped minus-type fraction  $F_{-,trap}$  and minus-type fraction  $F_-$  at the tip between lane-change protocols PI and PII. This shows for protocol PI that there are lower  $F_-$  and  $F_{-,trap}$  even for a similar mean tip size. When  $\alpha_+ > \alpha_c$  in both protocols,  $F_{-,trap} \approx 100\%$  and mean tip size does not convergent with time; marked as “–”. Other parameters are default as in Table 2 and boundary conditions as in (5).

	$\alpha_+(s^{-1})$	0.8	1	1.2	1.4	1.6	1.8	2.0	4
PI	$F_{-,trap}$	37.8%	49.0%	66.7%	72.5%	79.6%	85.7%	88.2%	99.7%
	$F_-$	3.7%	4.5%	5.7%	7.6%	9.4%	12.1%	14.3%	51.3%
	$\langle n_{tip} \rangle$	19.7	24.9	31.0	36.8	43.7	52.1	59.9	–
PII	$F_{-,trap}$	59.7%	83.3%	89.8%	92.6%	95.8%	98.5%	99.6%	100%
	$F_-$	5.4%	9.9%	14.3%	20.2%	28.6%	42.7%	50.4%	57.6%
	$\langle n_{tip} \rangle$	20.3	28.1	36.5	48.3	70.1	–	–	–

### 3.4. Measures of bidirectional transport efficiency

The previous subsections indicate that allowing minus-type particles to change lanes when incurring collision is more robust (say, against  $\alpha_+$ ) and effective (with less trapped minus-type particles) than allowing both type of particles to change lanes. To understand more on the bidirectional transport observed in living cells, it is interesting to speculate on the implications of the *in vivo* experiments data, particularly in Table 2, in terms of some non-trivial quantifiable efficiency.

There are many ways to define a quantitative notion of efficiency of bidirectional transport, depending on what sort of behaviour one wishes to highlight. For example, in some circumstances it could be that maximum speed is required (e.g., for signalling a threat to a cell) while in other circumstances it could be the maximum flux is required (for example, efficient transport of cell volume) - for a practical system of bidirectional transport on a MT, different notions may be needed for different purposes.

We define here two notions of transport efficiency based on the motion of the particles. Suppose that the  $n$ -th particle injected at the minus end is at location  $(l, i) = (L_n(t), I_n(t))$  at time  $t$ , and suppose:

- It enters the system at time  $t_{n,1}$  and leaves the system at time  $t_{n,4}$ .
- The farthest point it reaches into the system is  $d_n$ , i.e.  $d_n = \max_t I_n(t)$ .
- It enters the “tip” at time  $t_{n,2}$ , i.e. this is the smallest  $t$  such that  $I_n(t) > L_{tip}$ .
- It leaves the “tip” at time  $t_{n,3}$ , i.e. this is the largest  $t$  such that  $I_n(t) > L_{tip}$ .

where  $L_{tip}$  refers to the farthest site away from the plus end at the tip, typically we set  $L_{tip} \approx 90\%N$  for simulations. These times are illustrated in Figure 5 (left panel) with a comparison of endosome motility *in vivo* in Figure 5 (right panel). If the particle does not reach the tip then we have only  $t_{n,1} < t_{n,4}$  defined, while if  $d_n \geq L_{tip}$  then we have  $t_{n,1} < t_{n,2} < t_{n,3} < t_{n,4}$  defined. We define the dimensionless *particle arrival efficiency*

(arrival proportion) to be  $\parallel$

$$E_1 = \lim_{T \rightarrow \infty} E_1(T) = \lim_{T \rightarrow \infty} \frac{\#\{n : d_n \geq L_{tip}, t_{n,4} < T\}}{\#\{n : T_0 < t_{n,1} < t_{n,4} < T\}}.$$

It can be approximated by  $E_1(T)$  for long enough time  $T$ , which is approximately one (resp. zero) if majority (resp. minority) of particles reach the tip. Meanwhile, we define *average tip delay* (in unit of time) to be

$$E_2 = \lim_{T \rightarrow \infty} E_2(T) = \lim_{T \rightarrow \infty} \frac{\sum_{\{n : \|d_n\| \geq L_{tip}, t_{n,4} < T\}} (t_{n,3} - t_{n,2})}{\#\{n : d_n \geq L_{tip}, t_{n,4} < T\}}$$

which can be similarly approximated by  $E_2(T)$  for large enough time  $T$ .

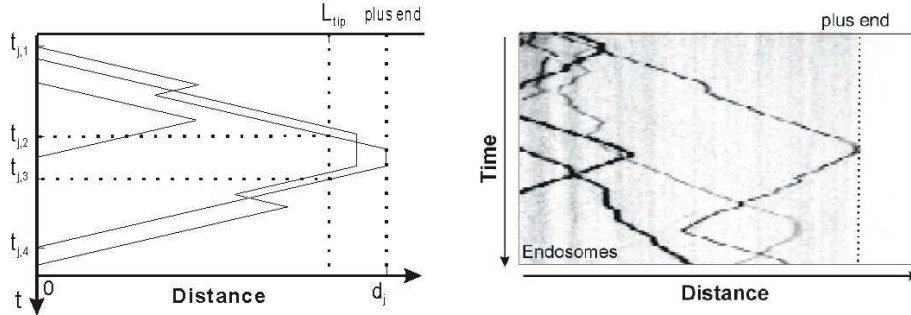


**Figure 5.** Typical motion of three particles injected into the system (left panel). We show the times  $t_{j,m}$   $m = 1, \dots, 4$  for the  $j$ -th particle. Particles that exceed  $L_{tip}$  are said to have entered the tip region. Kymograph (right panel) shows motility of early endosomes that were visualized by photo-activation of the endosome marker *paGFP-Rab5a* [15] in subapical regions of a cell of the fungus *Ustilago maydis*. Note the similarities in the two panels on the trajectories of motions.

The arrival efficiency is independent on the particle-type change rate from Figure 6(a) and Table 5 and we give approximate upper and lower bounds for  $E_1$  here. Considering the density of plus-type particles in dilute situation; see density approximation (A.3) in Appendix A.2, we have

$$\begin{aligned} E_1 &\leq \min\{\rho(1)/\rho(0), 1\} \\ &= \min\left\{\exp\left[\frac{Np_{-+}}{p_{-} + p_{+,u}^{\downarrow} + p_{+,u}^{\uparrow}} - \frac{Np_{+-}}{p_{+} + p_{+,u}^{\downarrow} + p_{+,u}^{\uparrow}}\right], 1\right\} \end{aligned} \quad (7)$$

while considering the probability of first particle-type change occurring at the tip, we have

$$E_1 \geq \left[1 - \frac{p_{+-}}{p_{+} + p_{+,u}^{\downarrow} + p_{+,u}^{\uparrow}}\right]^{L_{tip}} \approx 1 - \frac{Np_{+-}}{p_{+} + p_{+,u}^{\downarrow} + p_{+,u}^{\uparrow}} \quad (8)$$

as particles may change directions (type changes) several times before reaching the tip. Figure 6 (a) shows the upper and lower bounds for  $E_1$  compared to the simulations.

$\parallel$   $T_0$  is the time when we assume that the system is in a stationary state and particles' behaviour are recorded after that time, i.e.,  $t_{1,1} \geq T_0$ .

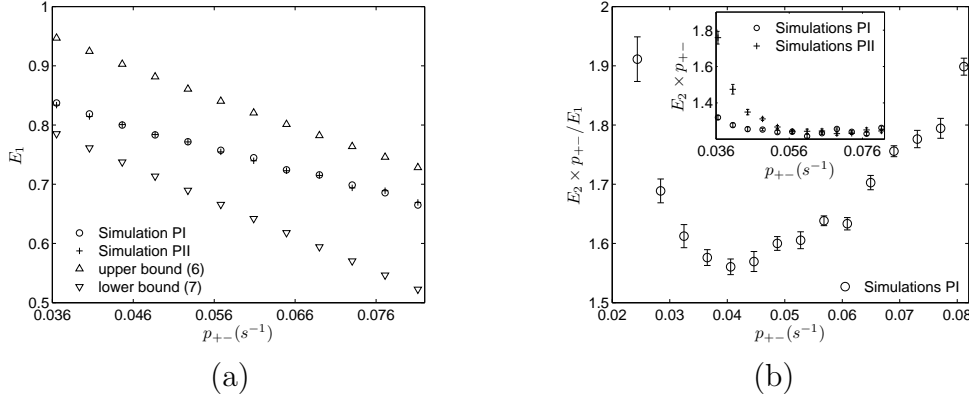


**Figure 6.** Illustration of  $E_1$  and  $E_2$  when varying  $p_{+-}$ . (a) shows the arrival efficiency  $E_1$  in both lane-change protocols PI and PII behaves similarly as varying  $p_{+-}$  with approximate upper bound from (7) and lower bound from (8). (b) shows the balance between delay ratio and arrival efficiency quantified as  $E_2 \times p_{+-} / E_1$  for protocol PI; the inset shows the comparison between two protocols PI and PII of the delay ratio  $E_2 \times p_{+-}$ ; errorbars are indicated. Simulations are done by averaging over 10 runs using the Gillespie algorithm in a time interval  $[T_0, T] = [500s, 3000s]$ ; other rates are default as in Table 2 and boundary conditions in (5).

The average tip delay  $E_2$  is clearly dependent on  $p_{+-}$  as  $1/p_{+-}$  is the expected delay of minus-type particles without obstruction such as in the two-lane model recalled in Section 2.1 (see [14] for details). We therefore consider the *delay ratio*  $E_2 \times p_{+-}$  (i.e. the ratio of the average tip delay to the expected delay if there are no trapped minus-type particles).  $E_2 \times p_{+-} = 1$  indicates the most efficient in terms of delay ratio. From Table 4, there is certain proportion of minus-type particles “trapped” at the tip in the thirteen-lane model, meaning that  $E_2 > 1/p_{+-}$ , i.e., the delay ratio  $E_2 \times p_{+-} > 1$ . This is confirmed in Table 5 and the inset to Figure 6. Comparing the Figure 6 (a) and the inset in Figure 6 (b), we consider the dimensionless quantity  $E_2 \times p_{+-} / E_1$  to be a balance between arrival efficiency and delay ratio. As varying  $p_{+-}$  and we find a minimum value where  $p_{+-}$  is closed to the experiment date of  $p_{+-} = 0.0406 s^{-1}$ ; see Figure 6 (b). This offers an implication of *in vivo* transport rates which leads to the discussion in Section 5.

Comparing the two lane-change protocols PI and PII, protocol PI is more effective in the sense that it has a relatively lower delay ratio  $E_2 \times p_{+-}$  when varying  $\alpha_+$  (see Table 5) or for small  $p_{+-}$  (see the inset in Figure 6 (b)). Similar to the case for trapped minus-type fraction and mean tip size, the average tip delay time increases more rapidly with injection rate in protocol PII than the increase in protocol PI.

#### 4. Critical behaviour and pulsing states

Results from Section 3.2 suggest that the mean tip size does not converge when an injection rate  $\alpha_+$  approaches a critical injection rate  $\alpha_{c,I}$  for lane-change protocol PI ( $\alpha_{c,II}$  for protocol PII) in a finite system; additionally, by simulating the efficiency

**Table 5.** Comparison of  $E_1, E_2$  between lane-change protocols PI and PII. The arrival efficiency  $E_1$  in both protocols is relatively independent of  $\alpha_+$  and drops to almost zero when  $\alpha_+ > \alpha_{c,I}$  for protocols PI ( $\alpha_+ > \alpha_{c,II}$  for protocol PII). The average tip delay  $E_2$  in both protocols are larger than the expected delay time  $1/p_{+-} \approx 24.6 \text{ s}^{-1}$  when no minus-type particles are trapped, and the delay time increases more rapidly for protocol PII than for PI when increasing  $\alpha_+$ . Note particle-type change rate  $p_{+-}$  is fixed here, meaning that the delay ratio  $E_2 \times p_{+-}$  is just a multiplication of a constant to the above  $E_2$ . Simulations are done as in Figure 6 with otherwise default parameters.

	$\alpha_+ (s^{-1})$	0.8	0.9	1	1.1	1.2	1.3	1.4	2
PI	$E_1$	81.9%	81.9%	81.5%	81.9%	81.6%	81.6%	81.9%	81.7%
	$E_2 \text{ (s)}$	30.71	30.87	31.1	31.1	31.8	32.6	33.5	48.8
PII	$E_1$	81.4%	81.8%	81.7%	81.7%	81.9%	81.8%	81.5%	$\approx 0$
	$E_2 \text{ (s)}$	31.9	33.2	34.2	37.9	44.9	48.7	61.4	–

defined in terms of delay ratio  $E_2 \times p_{+-}$ , the system will be less efficient with either a large total injection rate  $\alpha_+$  (see Table 5) or a small particle-type change rate  $p_{+-}$  (see Figure 6(b)). Large mean tip size or inefficiency on  $E_2 \times p_{+-}$  are expected due to high mixed densities of plus- and minus-type particles, and in the following we discuss the dynamics of pulsing states that exist in this model at high mixed densities.

#### 4.1. Pulsing states in the system

For injection rate  $\alpha_+$  smaller than the critical value  $\alpha_c$  discussed in Section 3.2, the system converges to a stationary state with an accumulation of certain size at the tip, and this tip size increases as  $\alpha_+$  approaching  $\alpha_c$ . For  $\alpha_+ > \alpha_c$  and otherwise default parameters, a new type of behaviour that we call *pulsing state* appears. These are characterized by the behaviour in Figure 7, shown for injection rate  $\alpha_+ = 4 \text{ s}^{-1}$  with otherwise rates as in Table 2 and boundary conditions in (5). For finite systems, near  $\alpha_c$  the accumulation may show large irregular oscillations including a propagating region or *pulse* of high density that moves away from the tip before dispersing.

In a **pulsing state**, the whole system density undertakes large approximately periodic oscillations. These can be split into two parts:

- A **filling phase** during which the density at the minus end is low, and a growing high density **pulse** of mixed particles moves steadily towards the minus end. During this phase there is a net flux into the system.
- An **emptying phase** during which the density at the minus-end is high, and the pulse propagates out of the system. During this phase there is a net flux out of the system.

For most of the cycle there is a low density region between the tip and the pulse. The pulsing occurs through an alternation between these phases as fronts (evident in Figure 7) separating low and high density regions move through the domain.



To better understand the behaviour of system in a pulsing state, Figure 8 shows as successive horizontal lines the evolution of the medium time average of the density  $\tau_{-,i} + \tau_{+,i}$  (over successive blocks of 1260 s) from a time-series and gradually changes of the local density. Figure 8 (a,b) shows rapid convergence to a stable accumulation at the tip, though (b) displays more fluctuations. Examples of pulsing states are illustrated in Figure 8 (d,e,f) for increasing values of  $\alpha_+$ ; these exhibit long approximately periodic oscillations. Figure 8 (c) shows an intermediate situation where the tip accumulation shows irregular large amplitude oscillations. The main behaviour in an extended high-density region will be change of particle type and therefore we expect the ratio of density between minus- and plus-type particles to reach the equilibrium ratio given by the type-change rates, i.e.

$$\tilde{\rho} = \frac{p_{-+}}{p_{-+} + p_{+-}}\kappa, \quad \tilde{\sigma} = \frac{p_{+-}}{p_{-+} + p_{+-}}\kappa$$

where  $\kappa = \tilde{\rho} + \tilde{\sigma} \approx 1$  represents the total local density.

For both lane-change protocols PI and PII we find pulsing states for  $\alpha_+ > \alpha_c$  and otherwise default parameters - we interpret this as an existence of a negative net flux for the high-density mixed phase. If  $\tilde{\rho}_u$  represents the density of plus-particles within the high density region that are not blocked and  $\tilde{\rho}_b$  the density of plus-type particles that are blocked but can move by changing lanes (similarly  $\tilde{\sigma}_{u,b}$ ), assuming the density of particles doing lane changes when unblocked is much smaller than  $\tilde{\rho}_u$  (this is possible if  $p_{\pm,u} \ll p_{\pm}$  in high-density mixed state), then the net flux  $j$  of particles to the right can be approximated to be

$$j \approx p_+ \tilde{\rho}_u + (p_{+,b}^{\downarrow} + p_{+,b}^{\uparrow}) \tilde{\rho}_b - p_- \tilde{\sigma}_u - (p_{-,b}^{\downarrow} + p_{-,b}^{\uparrow}) \tilde{\sigma}_b. \quad (9)$$

Note that densities  $\tilde{\rho}, \tilde{\sigma}$  are primarily governed by the particle-type change rates  $p_{+-}, p_{-+}$ , if we increase  $p_{-+}$ , then net flux  $j$  may change to be positive and the pulsing state is replaced by approaching to a high-density uniform *filled state*. For example, Figure 9 (a) shows the pulsing state for  $p_{-+} = 0.05 \text{ s}^{-1}$  with  $\alpha_+ = 3 \text{ s}^{-1}$  while Figure 9 (b) shows a filled state for  $p_{-+} = 0.14 \text{ s}^{-1}$  and  $\alpha_+ = 4 \text{ s}^{-1}$  (other parameters are the default values). For the latter case, we infer that an initial pulse with  $j > 0$  will saturate to  $\tilde{\rho} + \tilde{\sigma} = 1$  and then  $j \rightarrow 0$  as the number of vacancies in the high density state goes to zero. It will be an interesting challenge to understand the statistical properties of these high-density mixed states and, for example, to predict  $j$  from the parameters of the system.

#### 4.2. A simple model with a critical injection rate

To better understand the appearance of a critical injection rate  $\alpha_+ = \alpha_c$  that leads to unbounded growth of the tip, we discuss a simple model that computably predicts nonlinear behaviour of tip size with injection rate  $\alpha_+$ , and a singularity of the tip size at finite injection rate.

Consider a single lane first-in, last-out queue of plus-type and minus-type particles. Plus-type particles are assumed to arrive at the left end of the queue at a rate  $\alpha$  per

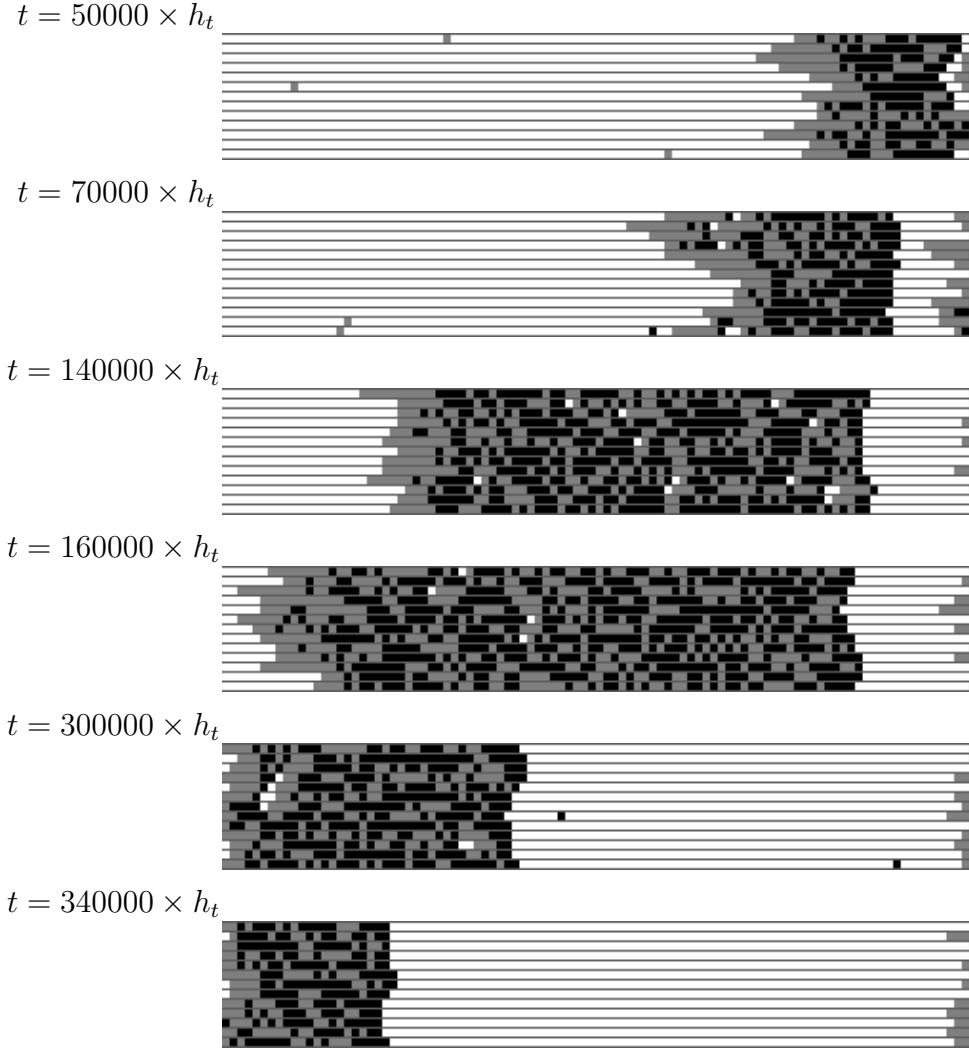


**Figure 7.** Time progress of a pulsing state for the thirteen lane model of size  $N = 100$ ,  $\alpha_+ = 4.0 \text{ s}^{-1}$  and no flux on the plus-end; otherwise parameters as in Table 2 and boundary conditions as in (5). The sequence of filling (top three frames) and emptying (bottom three frames) repeats approximately periodically. Observe the pulse of high-density mixed particles propagates slowly to the left via diffusion of vacancies through the pulse. Grey indicates plus-type particles (that move to the plus end with given rate if there is a vacancy) while black indicates minus-type particles that move to the left - the white regions are vacancies.

time-step. Every time-step, we assume that all particles independently to be minus-type with probability  $p$  and plus-type with probability  $1 - p$ . A number of particles is assumed to leave the queue whenever the left-most particle is of minus-type, in which case all of the adjacent particles of minus-type are assumed (instantaneously) to leave the queue. This results in a steady growth and intermittent loss of particles. At a given time-step  $t$ , if we assume the queue has size  $n(t)$  then after the random changes in type,

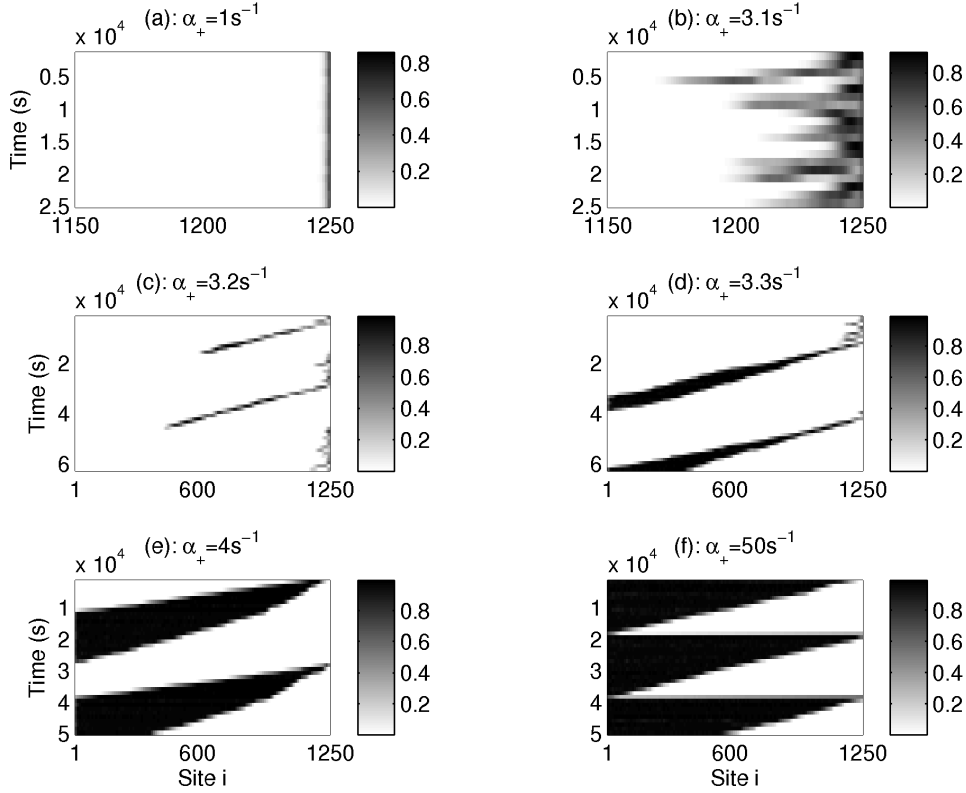


**Figure 8.** Each horizontal line represent a time-average of the occupancy  $\sum_{l=1}^M (\tau_{+,i}^l + \tau_{-,i}^l)/M$  over blocks of length 1260 s in the homogeneous thirteen-lane model ( $M = 13$ ) with injection rate  $\alpha_+$  indicated (other rates as default). In (a), the model with a small total injection rate reaches its stationary state with a small number of particles accumulated in the tip. (b)-(d) show the density-time courses for injection rates near the critical value. In (d)-(f), pulsing states appear where the tip accumulation moves away from the plus end and simultaneously grows.

the number of particles that leave the queue can be expressed as

$$\lambda(n) = \sum_{m=1}^n m p^m (1-p) + n p^n = p \frac{1-p^n}{1-p}.$$

Hence the mean rate of net growth of the queue will be given by  $\alpha_+ - \lambda(n)$ . This will give zero mean growth when  $\alpha_+ - \lambda(n) = 0$ . Therefore, with injection rate  $\alpha_+$ , the mean size of the queue is

$$\langle n(\alpha_+) \rangle = \frac{\ln \left( 1 - \alpha_+ \frac{1-p}{p} \right)}{\ln p},$$

which predicts a critical injection rate  $\alpha_c = \frac{p}{1-p}$ . For  $\alpha_+ < \alpha_c$ ,  $\langle n(\alpha_+) \rangle$  grows monotonically and nonlinearly with  $\lim_{\alpha_+ \rightarrow \alpha_c^-} \langle n \rangle(\alpha) = \infty$ . For  $\alpha_+ > \alpha_c$  the model predicts an unbounded growth of the queue. These are clear analogies with the observations of tip size in the thirteen-lane model in Figure 3. Indeed, one can fit

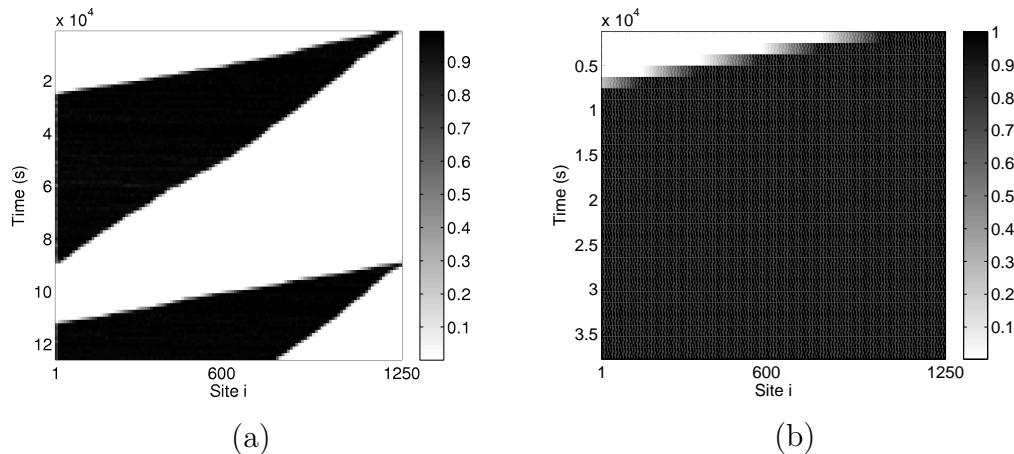


**Figure 9.** (a) shows a pulsing state for  $p_{-+} = 0.05 \text{ s}^{-1}$  and  $\alpha_{+} = 3 \text{ s}^{-1}$ ; (b) shows a “filled” state for  $p_{-+} = 0.14 \text{ s}^{-1}$  and  $\alpha_{+} = 4 \text{ s}^{-1}$  and this approaches a homogeneous high-density equilibrium state. The other rates are default as in Table 2 and boundary conditions in (5).

the data in Figure 3 to a logarithmic function but the fit is inferior to the rational function discussed there, suggesting that the model above is too simple for an accurate quantitative explanation.

## 5. Discussion

Motor-driven bidirectional transport of organelles is vital for the organization and function of eukaryotic cells and intracellular motility serves numerous cellular processes [24] - we start with a discussion of the relevance of our model as a description of this cellular process. The basic function of bidirectional vesicle transport is to deliver cargo over distances, thereby modifying gradients and ensuring communication between different regions of a cell. By considering the process in a number of stages, starting with cargo uptake, followed by transport along the fibres of cytoskeleton, and finally ending with cargo off-loading, the site of unloading is often also a region of cargo uptake. Transport back on the cytoskeletal track therefore not only recycles the transport vesicles, but also serves for long-distance delivery to other regions of the cell.

Using a fungal model system, it has recently been shown that dynein are concentrated at MT plus-ends to prevent organelles falling off the track and this concentration of dynein is done by an active retention mechanism (based on controlled protein-protein interaction) and stochastic motility of motors [15, 25]. However, the accumulation of motors at MT plus-ends can be seen as an inefficiency, as dynein motors are supposed to transport particles rather than wait at the MT end. Thus, the cell needs to find a compromise between (a) ensuring that organelles are captured at MT ends, which requires dynein accumulation at the plus-ends [15] and (b) keeping dynein moving along MTs to deliver the cargo to minus-ends.

In this paper, we consider the thirteen-lane model of [15] recalled in Section 2.2

where plus-type particles represent dynein carried by kinesin-1 while minus-type particles represent dynein carrying kinesin-1 and consider the effect of changes in parameters. To address the above compromise between (a) and (b), we consider the influence of varying the particle-direction change rate  $p_{+-}$  in the model. This rate is related to the “tug-of-war” [21, 20, 22] between opposing motors (kinesin-1 and dynein) to bind to the MT. Figure 6 shows that decreasing  $p_{+-}$ , on one hand increases the arrival proportion of particles (related to (a)) while on the other hand it increases the ratio of delay (related to (b)). Interestingly, Figure 6 (b) shows that the rate  $p_{+-} = 0.0406 \text{ s}^{-1}$  obtained from experiments is close to optimal for the biologically realistic system with parameters in Table 2 in the sense that it provides an a good balance between these. By comparing different lane-change rules (that is, either dynein changes lanes or both kinesin-1 and dynein change lanes), we find that allowing only dynein to change lanes gives biologically realistic system states over a larger range of possible fluxes; see Figure 3.

It is natural to compare the flux of transport we find in the thirteen-lane model with the possibly maximum unidirectional flux in the same model. By analogy with the so-called *maximal current state* in the ASEP model [3, 4], the maximum unidirectional flux in the thirteen-lane system occurs when  $\alpha_+ \approx 6 \times p_+/2 \approx 600 \text{ s}^{-1}$ , assuming appropriate boundary conditions and rates that separate different particles type in different lanes (as in Table 1). However, the existence of the critical injection rate  $\alpha_c \ll 600 \text{ s}^{-1}$  (see Figure 3) in a half-closed system (no flux on the plus end) places a much lower bound on the maximum unidirectional flux and the experimentally measured  $\alpha_+ \approx 1.06 \text{ s}^{-1}$  in Table 2 is of the same order as  $\alpha_c$ . To achieve the maximum unidirectional flux for the particles in the transport on a MT, much more organized transport (with very specific controlling of lane-change and turning behaviour) is therefore necessary. For  $\alpha_+ > \alpha_c$  we have described novel “pulsing states” of the system. It will be very interesting to further explore whether there exist new phases for other boundary conditions and transition rates in the multi-lane model.

To make a more realistic model for MT transport, other parameters known to affect transport along MTs would need to be included. In particular, (a) more species of motor with different transport properties need to be considered, as experimental evidence shows that MTs are utilized by several types of kinesin *in vivo* [1, 26] and these motors are expected to increase collisions along the MT length; (b) the possibility of detachment and reattachment of motors from the MT [9] needs to be taken into account; (c) non-trivial geometry of MT bundles needs consideration as motors may jump between different MTs; (d) a realistic motor size will influence the ability of lane changes to overcome blockages, and finally (e) static obstructions such as MAPs (microtubule associated proteins) will influence the behaviour of motors on the MT [27, 28, 29, 18]. At present, quantitative data for most of these parameters in the living cell are not available. With each aspect added to the model, we will gain a more quantitatively precise mathematical representation of the full MT-mediated transport within a cell. It remains to be seen whether new qualitative effects will also appear for

more accurate models.

## Acknowledgments

We thank Martin Schuster for acquiring the images that were used to generate the kymograph shown in Figure 5 (right panel).

## References

- [1] Vale R D, 2003 *Cell* **112** 467
- [2] Tilney L G, Bryan J, Bush D J, Fujiwara K, Mooseker M S, Murphy D B and Snyder D H, 1973 *J. Cell Biol.* **59** 267
- [3] Derrida B, Evans M R, Hakim V and Pasquier V, 1993 *J. Phys. A: Math. Gen.* **26** 1493
- [4] Blythe R A and Evans M R, 2007 *J. Phys. A: Math. Thero.* **40** R333
- [5] Parmeggiani A, Franosch T and Frey E, 2003 *Phys. Rev. Lett.* **90** 086601
- [6] Popkov V, Rákos A, Willmann R D, Kolomeisky A B and Schütz G M, 2003 *Phys. Rev. E* **67** 066117
- [7] Kolomeisky A B, Schütz G M, Kolomeisky E B and Straley J P, 1998 *J. Phys. A: Math. Gen.* **31** 6911
- [8] Muhuri Sand and Pagonabarraga I, 2008 *EPL* **84** 58009
- [9] Ebbinghaus M and Santen L, 2009 *J. Stat. Mech.* P03030
- [10] Ebbinghaus M, Appert-Rolland C and Santen L, 2010 *Phys. Rev. E* **82** 040901
- [11] Liu M Z, Xiao S and Wang R L, 2010 *Mod. Phys. Lett. B* **24** 707
- [12] Juhász R, 2007 *Phys. Rev. E* **76** 021117
- [13] Juhász R, 2010 *J. Stat. Mech.* P03010
- [14] Ashwin P, Lin C and Steinberg G, 2010 *Phys. Rev. E* **82** 051907
- [15] Schuster M, Kilaru S, Ashwin P, Lin C, Severs N J and Steinberg G, 2011 *EMBO J.* **30** 652
- [16] Wang Z, Khan S and Sheetz M P, 1995 *Biophys. J.* **69** 2011
- [17] Ray S, Meyhöfer E, Milligan R A and Howard J, 1993 *J. Cell Biol.* **121** 1083
- [18] Dreblow K, Kalchishkova N and Böhm K J, 2010 *Biochem. Biophys. Res. Commun.* **395** 490
- [19] Müller M J I, Klumpp S and Lipowsky R, 2008 *Proc. Natl. Acad. Sci. U.S.A.* **105** 4609;
- [20] Müller M J I, Klumpp S and Lipowsky R, 2010 *Biophys. J.* **98** 2610;
- [21] Hendricks A G, Perlson E, Ross J L, Schroeder H W 3rd, Tokito M, Holzbaur E L, 2010 *Curr. Biol.* (pub ahead of print)
- [22] Soppina V, Rai A K, Ramaiya A J, Barak P and Mallik R, 2009 *Proc. Nat. Acad. Sci. USA* **106** 19381
- [23] Gillespie D T, 1977 *J. Phys. Chem.* **81** 2340
- [24] Welte M A and Gross S P, 2008 *HFSP J.* **2** 178
- [25] Schuster M, Lipowsky R, Assmann M A, Lenz P, Steinberg G, 2011 *Proc. Nat. Acad. Sci. USA* in press
- [26] Wedlich-Söldner R, Straube A, Friedrich M W and Steinberg G, 2002 *EMBO J.* **21** 2946
- [27] Seitz A, Kojima H, Oiwa K, Mandelkow E -M, Song Y -H and Mandelkow E, 2002 *EMBO J.* **21** 4896
- [28] Chai Y, Lipowsky R and Klumpp S, 2009 *J. Stat. Phys.* **135** 241
- [29] Telley I A, Bieling P and Surrey T, 2009 *Biophys. J.* **96** 3341

## Appendix A. Mean field approximation for the multi-lane model

We use a mean field approximation to give an equation for evolution of the densities  $\rho_i^l$  and  $\sigma_i^l$  for the multi-lane model with lane-homogeneous rates (but not necessarily boundary conditions). Examining the balance of incoming and outgoing particles to a given site, the mean field approximation gives the following, where on the right hand side we write  $\rho_i$  to mean  $\rho_i^l$ , etc.

$$\begin{aligned} \frac{d\rho_i^l}{dt} = & p_+\rho_{i-1}(1 - \rho_i - \sigma_i) + p_{-+}\sigma_i - p_+\rho_i(1 - \rho_{i+1} - \sigma_{i+1}) - p_{+-}\rho_i \\ & + p_{+,u}^\uparrow\rho_{i-1}^{l-1}(1 - \rho_i^{l-1} - \sigma_i^{l-1})(1 - \rho_i - \sigma_i) \\ & + p_{+,u}^\downarrow\rho_{i-1}^{l+1}(1 - \rho_i^{l+1} - \sigma_i^{l+1})(1 - \rho_i - \sigma_i) \\ & + \left(p_{+,b}^\uparrow\rho_{i-1}^{l-1}(\rho_i^{l-1} + \sigma_i^{l-1}) + p_{+,b}^\downarrow\rho_{i-1}^{l+1}(\rho_i^{l+1} + \sigma_i^{l+1})\right)(1 - \rho_i - \sigma_i) \\ & - \left(p_{+,u}^\uparrow(1 - \rho_{i+1}^{l-1} - \sigma_{i+1}^{l-1}) + p_{+,u}^\downarrow(1 - \rho_{i+1}^{l+1} - \sigma_{i+1}^{l+1})\right)\rho_i(1 - \rho_{i+1} - \sigma_{i+1}) \\ & - \left(p_{+,b}^\uparrow(1 - \rho_{i+1}^{l-1} - \sigma_{i+1}^{l-1}) + p_{+,b}^\downarrow(1 - \rho_{i+1}^{l+1} - \sigma_{i+1}^{l+1})\right)\rho_i(\rho_{i+1} + \sigma_{i+1}) \end{aligned}$$

There is a similar expression for  $\frac{d\sigma_i^l}{dt}$ , but for reasons of space we do not give this here. As the general mean field equations are not easy to solve, we consider below two special cases of these mean field equations.

### Appendix A.1. Dilute lane-inhomogeneous densities

Let us assume that

- $\rho_i^l(t) = \rho^l(x, t)$  with  $x = i\delta$  (where  $\delta = 1/N = h_s/L$  is small) and the spatial dimension is parametrized by  $x \in [0, 1]$ ,
- $\rho$  and  $\sigma$  are small (i.e. dilute limit);
- the lane changes rates are lane homogeneous and symmetric (i.e.,  $p_{\pm,u} = p_{\pm,u}^{\downarrow(\uparrow)}$ );

On expanding  $\rho_{i+1}^l = \rho^l(x) + \delta \frac{\partial \rho^l}{\partial x} + O(\delta^2)$  and discarding any terms that are quadratic in  $\delta$ , the mean field equations above simplify to

$$\begin{aligned} \frac{\partial \rho^l}{\partial t} = & -\delta p_+ \frac{\partial \rho^l}{\partial x} + p_{+,u} \left( \rho^{l+1} + \rho^{l-1} - 2\rho^l - \delta \frac{\partial \rho^{l-1}}{\partial x} - \delta \frac{\partial \rho^{l+1}}{\partial x} \right) \\ & + p_{-+}\sigma^l - p_{+-}\rho^l \\ \frac{\partial \sigma^l}{\partial t} = & \delta p_- \frac{\partial \sigma^l}{\partial x} + p_{-,u} \left( \sigma^{l+1} + \sigma^{l-1} - 2\sigma^l + \delta \frac{\partial \sigma^{l-1}}{\partial x} + \delta \frac{\partial \sigma^{l+1}}{\partial x} \right) \\ & + p_{+-}\rho^l - p_{-+}\sigma^l \end{aligned}$$

which can be used to characterize the combination of bidirectional transport ( $p_\pm$ ), change in direction ( $p_{+-}$  and  $p_{-+}$ ) and cross-lane diffusion ( $p_{\pm,u}$ ) on the density. Considering a region of the domain where the dilute approximation holds, the stationary

state distribution will therefore satisfy

$$\begin{aligned} \delta p_+ \frac{d\rho^l}{dx} &= p_{+,u} \left( \rho^{l+1} + \rho^{l-1} - 2\rho^l - \delta \frac{d\rho^{l-1}}{dx} - \delta \frac{d\rho^{l+1}}{dx} \right) + p_{-+}\sigma^l - p_{+-}\rho^l \\ -\delta p_- \frac{d\sigma^l}{dx} &= p_{-,u} \left( \sigma^{l+1} + \sigma^{l-1} - 2\sigma^l + \delta \frac{d\sigma^{l-1}}{dx} + \delta \frac{d\sigma^{l+1}}{dx} \right) \\ &\quad + p_{+-}\rho^l - p_{-+}\sigma^l. \end{aligned}$$

If  $p_{\pm,u} = 0$ , adding the above two equations gives  $p_+ \frac{d\rho^l}{dx} = p_- \frac{d\sigma^l}{dx}$ , meaning that in dilute situation,  $\rho$  and  $\sigma$  have a linear relationship. This gives a solution to the above ODEs:

$$\rho(x) = C \exp \left[ \left( \frac{p_{-+}N}{p_-} - \frac{p_{+-}N}{p_+} \right) x \right] + D \quad (\text{A.1})$$

$$\sigma(x) = \frac{p_+C}{p_-} \exp \left[ \left( \frac{p_{-+}N}{p_-} - \frac{p_{+-}N}{p_+} \right) x \right] + \frac{p_{+-}D}{p_{-+}} \quad (\text{A.2})$$

where  $C, D$  can be determined by the densities at  $\rho(x_0)$  and  $\sigma(x_0)$ .

If  $p_{\pm,u}$  are large ( $p_{+-}, p_{-+} \ll p_{\pm,u}$ ), ignoring the turning rates, the above ODEs lead to

$$\begin{aligned} \delta p_+ \frac{d\rho^l}{dx} &= p_{+,u} \left( \rho^{l+1} + \rho^{l-1} - 2\rho^l - \delta \frac{d\rho^{l-1}}{dx} - \delta \frac{d\rho^{l+1}}{dx} \right) \\ -\delta p_- \frac{d\sigma^l}{dx} &= p_{-,u} \left( \sigma^{l+1} + \sigma^{l-1} - 2\sigma^l + \delta \frac{d\sigma^{l-1}}{dx} + \delta \frac{d\sigma^{l+1}}{dx} \right). \end{aligned}$$

### Appendix A.2. Lane-homogeneous densities

Now consider homogeneous model which gives lane-homogeneous densities  $\rho(x) = \rho_i^l$  due to the symmetric structure of the cylinder and as before  $x = i\delta$ . In this case we have, ignoring second and higher order terms in  $\delta = 1/N$ , that the stationary state in the dilute case satisfies

$$\begin{aligned} 0 &= p_{-+}\sigma - p_{+-}\rho + \delta \left[ -p_+ - p_{+,u}^\uparrow - p_{+,u}^\downarrow \right] \frac{d\rho}{dx} \\ 0 &= -p_{-+}\sigma + p_{+-}\rho + \delta \left[ p_- + p_{-,u}^\uparrow + p_{-,u}^\downarrow \right] \frac{d\rho}{dx} \end{aligned}$$

Assuming zero net flux, this implies that  $v_+\rho - v_-\sigma = 0$  where  $v_\pm/h_s = p_\pm + p_{\pm,u}^\uparrow + p_{\pm,u}^\downarrow$ . Applying the boundary conditions  $\rho(0) = \frac{\alpha_+}{p_+M}$  gives

$$\rho(x) = \frac{\alpha_+}{p_+M} \exp \left[ \left( \frac{Np_{-+}}{p_- + p_{-,u}^\downarrow + p_{-,u}^\uparrow} - \frac{Np_{+-}}{p_+ + p_{+,u}^\downarrow + p_{+,u}^\uparrow} \right) x \right] \quad (\text{A.3})$$

analogous to the expression found for the two lane model in [14] but spread over all  $M$  lanes. This mean field approximation of density works well for low densities but near the tip, plus-type and minus-type particles do not have complementary density as in [14]; in fact they can be at the same order near the tip for typical turning rates; for this reason it does not appear to be easy to obtain the mean tip size from a mean field approximation.